von Willebrand disease type 2A phenotypes IIC, IID and IIE: A day in the life of shear-stressed mutant von Willebrand factor

Maria A. Brehm*[1]; Volker Huck*[4]; Camilo Aponte-Santamaría[3]; Tobias Obser[1]; Sandra Grässle[4]; Florian Oyen[1]; Ulrich Budde[2]; Sonja Schneppenheim[2]; Carsten Baldauf[5]; Frauke Gräter[3]; Stefan W. Schneider[4]; Reinhard Schneppenheim[1]

[1]Department of Paediatric Haematology and Oncology, University Medical Centre Hamburg-Eppendorf, Hamburg, Germany; [2]MEDILYS Laborgesellschaft mbH, Hemostaseology, Asklepios Klinik Altona, Hamburg, Germany; [3]Heidelberger Institut für Theoretische Studien, Heidelberg, Germany; [4]Heidelberg University, Medical Faculty Mannheim, Experimental Dermatology, Mannheim, Germany; [5]Fritz-Haber-Institut der Max-Planck-Gesellschaft, Berlin, Germany

Summary

The bleeding disorder von Willebrand disease (VWD) is caused by mutations of von Willebrand factor (VWF), a multimeric glycoprotein essential for platelet-dependent primary haemostasis. VWD type 2A-associated mutations each disrupt VWF biosynthesis and function at different stages, depending on the VWF domain altered by the mutation. These effects cause considerable heterogeneity in phenotypes and symptoms. To characterise the molecular mechanisms underlying the specific VWF deficiencies in VWD 2A/IIC, IID and IIE, we investigated VWF variants with patient-derived mutations either in the VWF pro-peptide or in domains D3 or CK. Additionally to static assays and molecular dynamics (MD) simulations we used microfluidic approaches to perform a detailed investigation of the shear-dependent function of VWD 2A mutants. For each group, we found distinct characteristics in their intracellular localisation visualising specific defects in biosynthesis which are correlated to respective multimer patterns. Using microfluidic assays we further determined shear flow-dependent characteristics in polymer-platelet-aggregate formation, platelet binding and string formation for all mutants. The phenotypes observed under flow conditions were not related to the mutated VWF domain. By MD simulations we further investigated how VWD 2A/IID mutations might alter the ability of VWF to form carboxy-terminal dimers. In conclusion, our study offers a comprehensive picture of shear-dependent and shear-independent dysfunction of VWD type 2A mutants. Furthermore, our microfluidic assay might open new possibilities for diagnosis of new VWD phenotypes and treatment choice for VWD patients with shear-dependent VWF dysfunctions that are currently not detectable by static tests.

Keywords

von Willebrand factor, VWD, shear flow, microfluidic, molecular dynamics simulations

Correspondence to:
Dr. Maria A. Brehm
Department of Paediatric Haematology and Oncology
University Medical Centre Hamburg-Eppendorf
Hs N21, Rm 111
Martinistrasse 52
20246 Hamburg, Germany
Tel.: +49 40 741058523, Fax: +49 40 741058931
E-mail: m.brehm@uke.de

* The first two authors contributed equally to this work.

Financial support:
This study was supported by research funding from the German Research Foundation (DFG) to the Research Group FOR1543: "Shear flow regulation of hemostasis – bridging the gap between nanomechanics and clinical presentation" (RS, MAB, TO, UB, VH, SWS, SG, CB, FG, CAS) and the SFB/Transregio23 (SWS TP A9).

Received: November 4, 2013
Accepted after major revision: February 11, 2014
Epub ahead of print: March 6, 2014

http://dx.doi.org/10.1160/TH13-11-0902
Thromb Haemost 2014; 112: 96–108

Introduction

von Willebrand factor (VWF) is a large multimeric glycoprotein that is essential for platelet-dependent primary haemostasis. VWF biosynthesis is initiated in the cytoplasm by production of the pre-pro-monomers that are further post-translationally modified within the endoplasmic reticulum (ER). Here, glycosylation occurs and dimerisation is facilitated by the formation of carboxy-terminal interchain disulphide bonds. These dimers are released to the Golgi apparatus where O-linked oligosaccharides are added. The pH-dependent assembly of mature high-molecular-weight multimers (HMWM) of VWF occurs in the trans-Golgi where dimers are multimerised by interchain disulphide bonds between the amino-terminal D'-D3 domains. After furin-cleavage in the trans-Golgi network (TGN) the VWF-propeptide remains non-covalently bound to mature VWF (1). VWF-HMWM then become organised in tubules which are subsequently stored in Weibel-Palade bodies (WPB) until stimulated release (1-3). In the circulation VWF reversibly transforms from an inactive globular to an active stretched conformation bound to the vessel wall and exposes the structural A1 domain for platelet adhesion (4-6). This is a pivotal step for platelet aggregation and subsequent blood clot formation at the site of vascular injury (7, 8). Mutations in the VWF coding gene cause VWD, an inherited bleeding disorder. Classification into types 1, 2 and 3 of VWD is based on the combined results of multiple static laboratory tests that determine VWF amount and activity as well as the relative amounts of large VWF multimers. VWD type 2 is further subclassified into 2A, 2B, 2M and 2N with respect to specific functional and structural defects. VWD type 2A can further be grouped according to their pat-

homechanism that leads to reduced VWF-HMWM. In patients with VWD type 2A phenotype IID, mutations in the CK domain of VWF affect C-terminal dimerisation, phenotype IIC describes VWF mutants that affect multimerisation and the phenotype IIE exhibits altered secretion (9).

Here, we address the multiple pathophysiologic mechanisms that are responsible for the heterogeneity of 2A/IIC, IID and IIE phenotypes. We investigated the mechanism by which mutations in defined VWF subdomains induce a certain defect in biosynthesis and function of VWF-HMWM which ultimately manifests in the resulting diverse VWD 2A phenotypes. We chose mutations which previously had been identified in VWD 2A patients and used confocal immunofluorescence microscopy to investigate their intracellular localisation by parallel visualisation of cellular sub-compartments. Furthermore, we ascertained their shear-dependent function by microfluidic determination of platelet binding characteristics, by a detailed investigation of their string formation pattern, and by characterisation of the impact of VWF mutations on polymer-platelet-aggregate formation. Furthermore, we performed molecular dynamics (MD) simulations to identify structural changes in the CK domain induced by VWD 2A/IID-associated mutations.

Methods

Immunofluorescence and confocal microscopy

Immunofluorescence was performed as previously described (10) 48 hours (h) post transfection. Antibodies used were: rabbit anti-VWF (DAKO, Glostrup, Denmark; 1:1,000), mouse anti-PDI (ER marker, abcam, Cambridge, UK, 1:100), mouse anti-Rab27a (Weibel-Palade-body marker, Santa Cruz, Santa Cruz, CA, USA; 1:50), mouse anti-GOLPH4 (cis-Golgi marker, Santa Cruz, 1:100), mouse anti-LAMP2 (Santa Cruz, 1:100), sheep anti-TGN46 (AbD Serotec, Puchheim, Germany; 1:100), goat anti-rabbit AF488 (Invitrogen, Carlsbad, CA, USA; 1:5,000), goat anti-mouse AF 546 (Invitrogen, 1:5,000), donkey anti-sheep AF 546 (Invitrogen, 1:5,000). For details on immunofluorescence, cell culture and expression of wild-type (wt) VWF and VWF mutants in HEK293 cells see Suppl. Methods (available online at www.thrombosis-online.com). Images were captured at room temperature (RT) with a confocal microscope (LSM 510; Carl Zeiss, Jena, Germany) using a Plan Apochromat 63×/1.4 oil DIC objective, ZEN 2009 software (Carl Zeiss), and the following settings: image size of 1776 × 1776 and 8 bit, laser power of the 543 and 488 nm lasers was set to 100% and 24%, respectively. After image capturing, the original LSM files were converted into TIFF files with the LSM Image browser software (Carl Zeiss).

Secretion of VWF and VWF:Ag-ELISA

In brief, HEK293 cells transiently expressing wtVWF or indicated mutants were treated with 160 nmol/l PMA. After indicated time points samples of the supernatant were taken, centrifuged (5 minutes [min] 13,000 xg, 4°C) and VWF concentration was determined by VWF:Ag-ELISA. Details are available in Suppl. Methods (available online at www.thrombosis-online.com).

Multimer analysis

Multimer analysis was performed as described (11-13). In brief, VWF multimers of recombinant VWF samples and patient's plasma were separated by SDS-agarose electrophoresis, transferred onto a nitrocellulose membrane and detected with anti-human VWF antibody-HRP linked (DAKO) and visualised by luminescence.

Structure modelling and molecular dynamics simulations of the VWF CK domain

The structure of the VWF CK domain (amino acids 2723-2813) was predicted by homology to the X-ray structure of the transforming growth factor-beta2 (TGFB2; Protein data bank ID code 2TGI) (14). These two proteins are cysteine-rich dimer-forming homologues and their sequences were aligned to match the cysteine residues, as previously proposed (15, 16). The structural modelling was carried out using the MOE software (Chemical Computing Group Inc. 2012, Molecular Operating Environment [MOE]), using the aligned sequences. During the modelling, internal-domain disulphide bonds found chemically (17) between the cysteine pairs Cys2724-Cys2774, Cys2739-Cys2788, Cys2750-Cys2804 and Cys2754-Cys2806 were considered as constraints. Remaining cysteines, Cys2771, Cys2773 and Cys2811, were kept unpaired. The resulting structure consisted of a CK dimer. This structure was fully solvated, energy minimised, and its side chains equilibrated through 1 ns of molecular dynamics (MD) simulations. After this procedure, one of the two CK domains was selected and used as the starting coordinates for further MD simulations. Equilibrium MD simulations were carried out for a fully solvated isolated CK domain, either in its wild-type form or by introducing the single amino acid mutations p.Cys2771Arg, p.Cys2773Arg or p.Ser2775Cys. MD simulations were carried out with the GROMACS package (18, 19) (4.5.5 version). Four simulations, each one lasting 140 ns, were carried out for the wild-type CK domain, as well as for the three considered mutants, yielding 16 independent simulations with a concatenated simulated time of 2.24 μs. A partial least squares functional mode analysis (PLS-FMA) (20) was carried out to identify mutation-induced structural changes of the CK domain which were correlated with VWF dimer abolishment determined experimentally. For all the parameters and algorithms employed in the simulations as well as a detailed explanation of the PLS-FMA method see the Suppl. Material (available online at www.thrombosis-online.com).

Microfluidic setup

For defined shear rate application, air-pressure driven microfluidic channels (BioFlux, San Francisco, CA, USA) with a width of 350 μm and a height of 70 μm were coated with wtVWF or VWF mutants (50 μg/ml) by application of 15 μl protein diluted in phosphate-buffered saline in one well and application of 5,000 s^{-1} for 4 s. After incubation over night at 37°C in a humidified environment the microfluidic channel system was mounted onto an inverted microscope (Zeiss Axio Observer Z.1, Zeiss AG, Oberkochen, Germany) capable of performing fluorescence- and reflec-

tion interference contrast microscopy (RICM). For the perfusion media, blood was collected from healthy volunteers using sodium citrated blood vacuum collection tubes. The study was conducted in conformity to the Declaration of Helsinki (21) and to *The International Conference on Harmonisation of Technical Requirements for Registration of Pharmaceuticals for Human Use (ICH)* Guidelines, available at http://www.ich.org, accessed in October 2010. It was approved by the *Ethics Committee of the Medical Faculty Mannheim*, Heidelberg University (Mannheim, Germany). Appropriate informed consent was obtained from all subjects.

In order to study the parameters platelet binding capability, string formation and rolling aggregate formation, three sets of experiments were designed and at least three independent experiments were performed.

- Channels coated with either wtVWF or indicated VWF mutants were perfused with washed and stained platelets in a concentration of 200,000 per µl as previously published (22) supplemented with 45% haematocrit at a shear rate of 500 s^{-1}. In accordance to the aforementioned protocol, note that any perfused components are intensively washed to exclude contamination by donor's VWF. After 10 min of perfusion, adhesion to the VWF-coated channel surface was studied by fluorescence microscopy and analysed using ImageJ (23) software for calculation of the surface coverage relative to wtVWF coated channels as previously published (24).
- To study string formation, channels were biofunctionalised with wtVWF and perfused with washed and Celltrace calcein-green (Invitrogen) stained platelets in a concentration of 200,000 per µl supplemented with 45% washed haematocrit at various shear rates in the range of 1,000 s^{-1} to 10,000 s^{-1} for 1 min each. Live cell fluorescence videos were taken with 4 frames/s and analysed as described. A video of wtVWF and mutant p.Cys2771Arg is available as Suppl. Video 1 (available online at www.thrombosis-online.com).
- To investigate rolling aggregate formation, channels were biofunctionalised with wtVWF and perfused with native whole

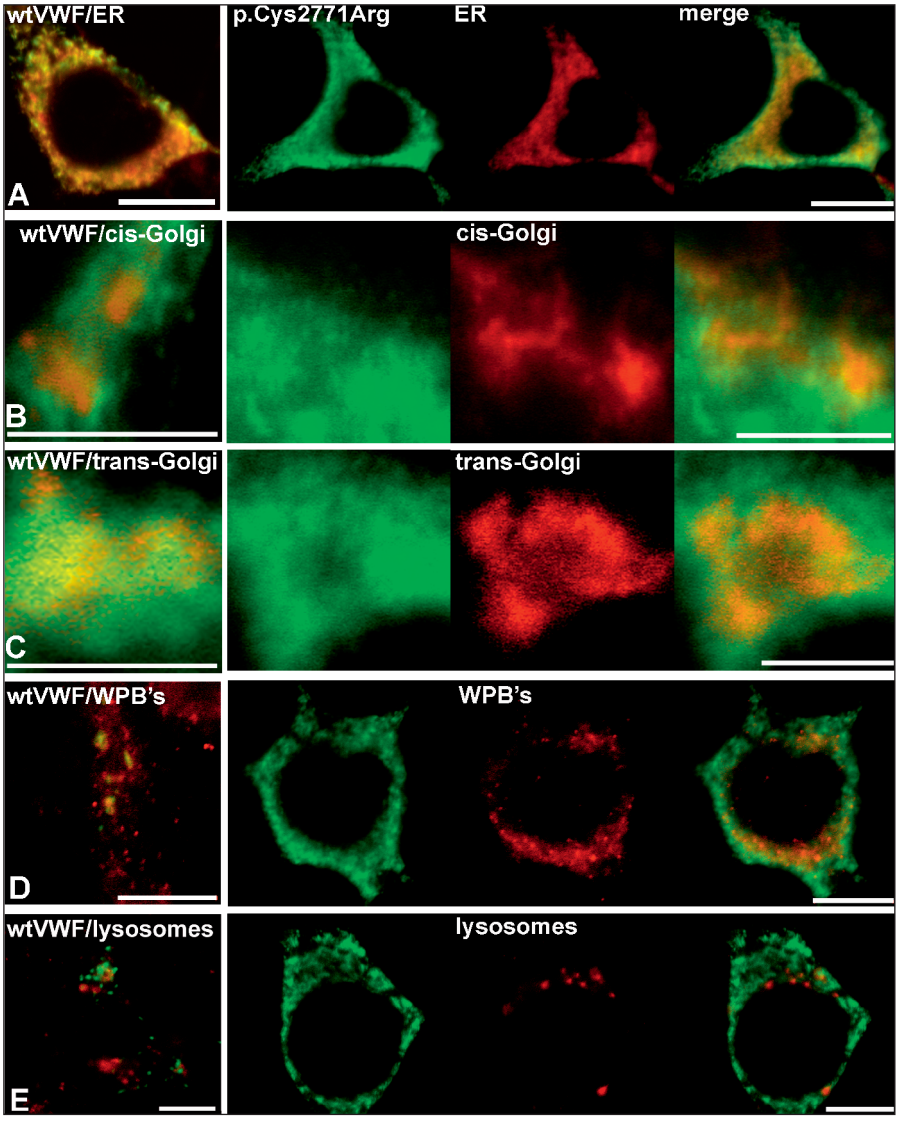

Figure 1: Intracellular localisation of VWD type 2A/IID inducing mutants in HEK293 cells. VWD 2A/IID inducing VWF mutant p.Cys2771Arg was transiently expressed in HEK293 cells. 48 h after transfection cells were fixed and p.Cys2771Arg as well as subcellular compartments were detected by indirect immunofluorescence employing anti-VWF and antibodies against marker proteins. Anti-PDI for the ER (A), anti-GOLPH4 for cis-Golgi (B), anti-TGN46 for trans-Golgi (C), anti-Rab27a for pseudo-Weibel-Palade bodies (D) and anti-LAMP2 for lysosomes (E). To illustrate altered ER and pseudo-WPB localisation of the mutants compared to wtVWF, the left-hand column shows an overlay of immunofluorescent detection of wtVWF and the indicated subcellular compartments. Three independent experiments for each mutant and for each subcellular compartment were performed. Scale bars represent 10 µm.

blood supplemented with either wtVWF or indicated VWF mutant to a concentration of 50 µg/ml. For determination of the critical shear rate, the flow was consecutively increased from 1,000 s^{-1} to 5,000 s^{-1} for 1 min each and live cell RICM videos were taken with 2 frames/s. Critical shear rate was defined as the shear rate at which the first rolling aggregates emerged that contained at least ~15 platelets. Videos of wtVWF and mutant p.Cys2773Arg are available as Suppl. Videos 2-4 (available online at www.thrombosis-online.com).

Statistical analysis

Mean data of experiments are given with standard deviation (SD). Statistical computation was performed with SAS 9.2 (SAS Institute Inc., Cary, NC, USA).

Results

Severity of the dimerisation defect of VWD type 2A/IID mutants

The biosynthesis of VWF-HMWM is a highly sophisticated process. Each step demands a spatial separation to ensure proper processing. We visualised each step by indirect immunofluorescence microscopy of wt and mutant VWF, transiently expressed in HEK293 cells, and marker proteins for the subcellular compartments that VWF passes during multimer formation.

We first investigated two patient-derived 2A/IID VWF variants with mutations in the CK domain: p.Cys2771Arg and p.Ser2775Cys. Compared to wtVWF (►Figure 1, left-hand column and Suppl. Figure 1, available online at www.thrombosis-online.com), the intracellular localisation of mutants p.Cys2771Arg and p.Ser2775Cys revealed a decrease in ER localisation (►Figure 1A (p.Cys2771Arg), Suppl. Figure 2, available online at www.thrombosis-online.com (p.Ser2775Cys)) meaning that less colocalisation with PDI was visible as seen by more green and less yellow in the overlay (►Figure 1A, right-hand panel) compared to wtVWF. Cis-Golgi (►Figure 1B) and the trans-Golgi network (►Figure 1C) localisation were not significantly altered compared to wtVWF. No normal cigar-shaped regular-sized pseudo-WPB's (wtVWF: ►Figure 1D, left-hand panel and Suppl. Figure 1B, E, available online at www.thrombosis-online.com) were formed by p.Cys2771Arg (►Figure 1D). Furthermore, these mutants did not show an increase in lysosome localisation (►Figure 1E). For a third VWD 2A/IID-associated mutant, p.Cys2773Arg (25), it has previously been shown that ER localisation, storage in pseudo-WPB's, and secretion is similar to wtVWF (26).

We next investigated if the extent of ER localisation was mirrored in the multimer size of the recombinant mutants homozygously expressed in HEK293 cells (►Figure 2). p.Cys2773Arg showed residual formation of small multimers with up to five bands and normal ER localisation, indicating residual formation of C-terminal dimers. These data are in accordance with previous observations by Wang et al. (26). Mutant p.Ser2775Cys exhibits

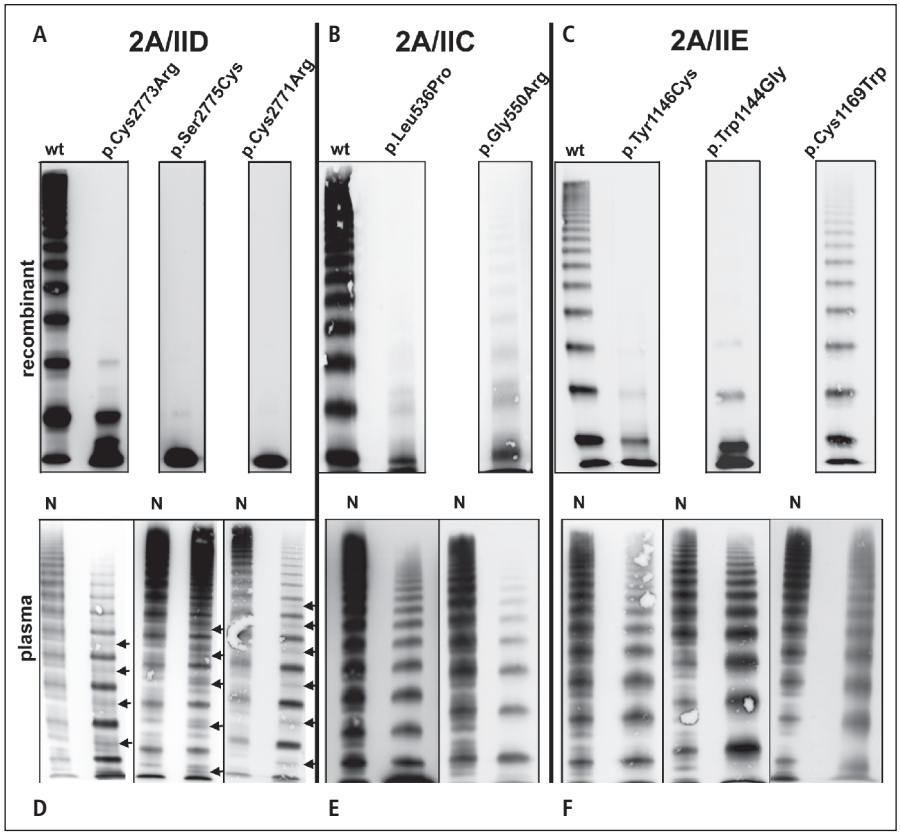

Figure 2: Multimer analysis of plasma-derived and recombinant VWF. Multimer analysis of recombinant VWD type 2A/IID (A), IIC (B), and IIE (C) mutants with indicated point-mutations and plasma derived VWF of patients with the same mutations (2A/IID (D), IIC (E), IIE (F)) was performed by SDS-agarose electrophoresis gels and immunoblotting onto nitrocellulose membrane with luminescent visualisation. The figure is composed of several gels. Black lines indicate separate gels. Recombinant wtVWF (wt) and normal plasma (N) was present on each gel. Additional bands in VWD 2A/IID patient plasma due to odd-numbered multimers are indicated by black arrows.

two bands along with reduced ER localisation. The mutant p.Cys2771Arg only presented one band in multimer analysis (►Figure 2A), indicating that no C-terminal dimerisation in the ER occurs, which might lead to the observed reduced ER localisation. Furthermore, heterozygous patients who carry the mutations p.Cys2771Arg, p.Cys2773Arg or p.Ser2775Cys on one allele exhibit odd-numbered bands in multimer analysis (black arrows, ►Figure 2D), presumably by attachment of monomers to wild-type multimers. Due to environmental circumstances the loss of VWF-HMWM can vary over time and between patients. Although loss of VWF-HMWM is less pronounced in the patient's plasma with mutation p.Ser2775Cys the bleeding symptoms persist indicating that the dimerisation defect is caused by a different mechanism in this mutant.

To explain the differences in the severity of the observed defects in multimer formation and trafficking in the IID mutants we performed molecular dynamics (MD) simulations of wt and mutated CK domain. It has previously been shown that residues Cys2771, Cys2773 and Cys2811 are unpaired in monomeric CK subunits and could therefore be used for intermolecular disulphide bonds facilitating dimerisation (17). We observed that mutation of Cys2771 leads to complete absence of multimers and alters ER localisation whereas mutant p.Cys2773Arg still forms small multimers and exhibits normal intracellular localisation.

To examine the structural basis for the distinct roles of cysteines in dimer formation, we created a structural model of the CK domain based on its homology with transforming growth factor (TGF)-β2 (►Figure 3A). In MD simulations of the wild-type CK domain model, we observed the disulphide-linked parallel segments of CK to be rigid (small root mean square fluctuation (RMSF), ►Figure 3A, blue/turquoise and Suppl. Figure 3, available online at www.thrombosis-online.com), whereas the loops and the C-terminus displayed higher flexibility (large RMSF, orange and red). [The recent crystal structure of the CK domain (27) validates the observed conformational dynamics of the CK domain, as discussed in Suppl. Material, available online at www.thrombosis-online.com][1].

We next analysed whether the single amino acid mutations p.Cys2771Arg, p.Cys2773Arg and p.Ser2775Cys lead to structural variations of the CK domain compared to the wild-type, by carrying out additional MD simulations of these mutants. We quantified the overall size of the CK domain by computing the radius of gyration r_g. All mutants appeared to induce structural deviations

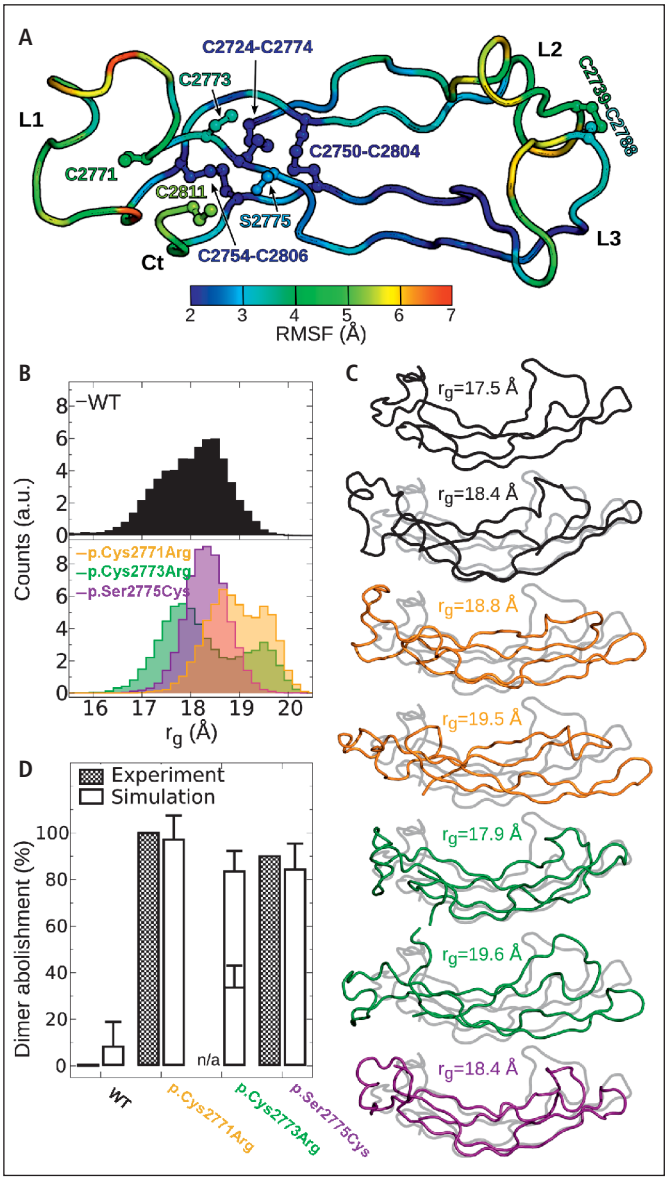

[1] Note added during proof.

Figure 3: Structure modelling and molecular dynamics (MD) simulations of the VWF CK-domain. A) Cartoon representation of a typical conformation sampled during the simulations. Loops are labelled as L1, L2 and L3 and the C-terminus with Ct. Cysteine residues, either unpaired or disulphide bonded, are labelled and depicted in ball-stick representation. The root mean square fluctuation (RMSF) per amino acid was derived from MD simulations. The RMSF quantifies the protein flexibility and is presented here colour-coded on the protein backbone trace according to the scale at the bottom. B) Histograms of the radius of gyration r_g as a measure of the overall size of the protein, obtained from MD simulations for the indicated forms of the CK domain (wild-type in black and mutants in colour). C) CK domain structures for different radii of gyration. Structures are displayed in cartoon representation: two for the wild-type (black), two for the p.Cys2771Arg mutant (p.Cys2771Arg, orange), two for the p.Cys2773Arg mutant (p.Cys2773Arg, green), and one for the p.Ser2775Cys mutant (p.Ser2775Cys, magenta). The most compact conformation (r_g=17.5 Å) of the wild-type is superposed to all structures in grey for comparison. D) VWF dimer abolishment induced by mutations. Comparison between predicted dimer abolishment by simulation (white bars) and experimental observations (dotted bars). For the p.Cys2773Arg mutant, the experimental dimer abolishment was not available (indicated here as n/a), while in the simulations it presented a bimodal behaviour fluctuating between two values (indicated by the two overlapped bars). See Suppl. Material (available online at www.thrombosis-online.com) for details of the dimer abolishment estimation from simulations.

from the wild-type (compare black with colour histograms in ►Figure 3B and black with colour structures in ►Figure 3C). CK mutants p.Cys2771Arg (orange) and p.Ser2775Cys (magenta) adopted extended conformations (as it is indicated by larger values of r_g) compared to the wt CK domain. p.Cys2773Arg fluctuated between extended and compact conformations (green).

We examined if dimer abolishment observed experimentally is correlated to dynamics underlying these structural differences among wild-type and mutant CK, by using partial least-squares functional mode analysis (20) (see details for this technique in Suppl. Methods and Suppl. Figure 4, available online at www.thrombosis-online.com). We detected dynamics of CK to be correlated with the ability of dimer formation observed in the experiments (►Figure 3D and Suppl. Figure 4, available online at www.thrombosis-online.com). We predicted conformational changes in the loops and the C-terminus to abolish dimer formation in mutant p.Cys2771Arg and mutant p.Ser2775Cys to 97% (10% SD) and 84% (11% SD), respectively, in good accordance with the experimental measurements. In addition, the p.Cys2773Arg mutant presented a bimodal behaviour, with the dimer abolishment alternating between two values, 34% (9% SD) and 83% (9% SD). We also monitored the separation between sulphur atoms of unpaired cysteines, $D_{S\text{-}S}$ (Suppl. Figure 5, available online at www.thrombosis-online.com). The sulphur atom of Cys2775 in the p.Ser2775Cys mutant was found with a high probability in proximity to the sulphur atom of Cys2773 and with moderate probability close to that of Cys2811. Introducing an additional cysteine in the p.Ser2775Cys mutant might therefore lead to alternate disulphide bonding within CK between cysteine residues that are not bridged by intramolecular disulphide bonds in wtVWF. Our data show that the extent of residual formation of small multimers and alteration in intracellular localisation is strongly correlated with simulated structural changes induced by the investigated mutations.

ER retention of VWD type 2A/IIC mutants

Phenotype IIC of VWD type 2A is caused by mutations within the pro-peptide of VWF which lead to reduced VWF-HMWM in the patient's plasma, indicating a multimerisation defect (28-30). We investigated two representative mutations (p.Leu536Pro and p.Gly550Arg) which we identified in VWD type 2A/IIC patients. VWF multimer analysis of the patients' plasma showed a reduction of HMWM in quantity and size (►Figure 2E). Similar effects were observed after recombinant expression in HEK293 cells (►Figure 2B). The reduction of HMWM of these mutants in the HEK293 cell supernatant was accompanied by an altered intracellular localisation. As shown exemplary for mutant p.Leu536Pro in ►Figure 4A, these mutants exhibit ER localisation only, whereas reduced colocalisation with trans-Golgi (►Figure 4C) was observed when compared to wtVWF (►Figure 4, left-hand column and Suppl. Figure 1, available online at www.thrombosis-online.com). Furthermore, no normal elongated pseudo-WPB's were detectable (►Figure 4D) and no obvious changes in cis-Golgi and lysosome localisation were observed (►Figure 4B, E). These data indicate retention of these mutants within the ER.

Weibel-Palade body retention of VWD type 2A/IIE mutants

We further analysed VWF multimer patterns of plasma samples from heterozygous patients with VWD type 2A/IIE carrying either D3 domain mutation p.Trp1144Gly (31), p.Tyr1146Cys, or p.Cys1169Trp (31) on one allele. All three mutants showed a moderate quantitative reduction of HMWM (►Figure 2F). In HEK293 cell supernatant the loss of HMWM was more severe for p.Tyr1146Cys and p.Trp1144Gly. Plasma and recombinant mutant p.Cys1169Trp (►Figure 2C) exhibited the same extent of HMWM reduction.

When compared to wtVWF (►Figure 5, left-hand column), we found normal localisation within the ER (►Figure 5A), cis- and trans-Golgi network (►Figure 5B,C) for all three mutants (►Figure 5 shows representative mutant p.Trp1144Gly). Strikingly, these mutants were highly enriched in pseudo-WPB's (►Figure 5D). No increase in lysosome localisation was observed (►Figure 5E).

These data indicated that these mutants are not prone to increased intracellular degradation but show an increase in storage. To further investigate a potential secretion defect we measured secretion of recombinant wtVWF and mutants p.Trp1144Gly, p.Tyr1146Cys and p.Cys1169Trp from HEK293 cells with and without PMA. As shown in Suppl. Figure 6 (available online at www.thrombosis-online.com), type 2A/IIE mutants exhibited decreased secretion compared to wtVWF without PMA treatment. Addition of PMA was sufficient to slightly increase secretion of mutants p.Trp1144Gly and p.Tyr1146Cys but to a much lesser extent than wtVWF. Only mutant p.Cys1169Trp could be released to the same extent as wtVWF. Normal secretion was observed for the p.Cys2771Arg control mutant (Suppl. Figure 6, available online at www.thrombosis-online.com).

Platelet binding capability of immobilised VWF mutants

It is well known that endothelial derived VWF is secreted to the subendothelial matrix as well as to the vascular lumen. To investigate if type 2A/IIC, IID and IIE mutations also alter VWF function in a shear flow environment, we mimicked the immobilised VWF exposed to the blood flow by biofunctionalisation of microfluidic channels with VWF mutants and characterised their platelet binding capability under laminar flow conditions. After 10 min of low-shear perfusion (500 s^{-1}) we quantified the platelet binding capability by the coverage of adhered platelets to the mutant coated surface normalised to the platelet surface coverage of 35 ± 3% (set to 100%) induced by wtVWF coating (►Figure 6A). The platelet surface coverage of type 2A/IIC VWD mutants p.Leu536Pro and p.Gly550Arg was nearly abolished. Mutant p.Cys2773Arg showed a platelet adhesion pattern comparable to wtVWF (94 ± 4% vs 100 ± 4%), whereas p.Ser2775Cys and p.Cys2771Arg failed to bind platelets under shear flow conditions. Also biofunctionalisation with the type 2A/IIE mutants p.Trp1144Gly and p.Cys1169Trp did not show

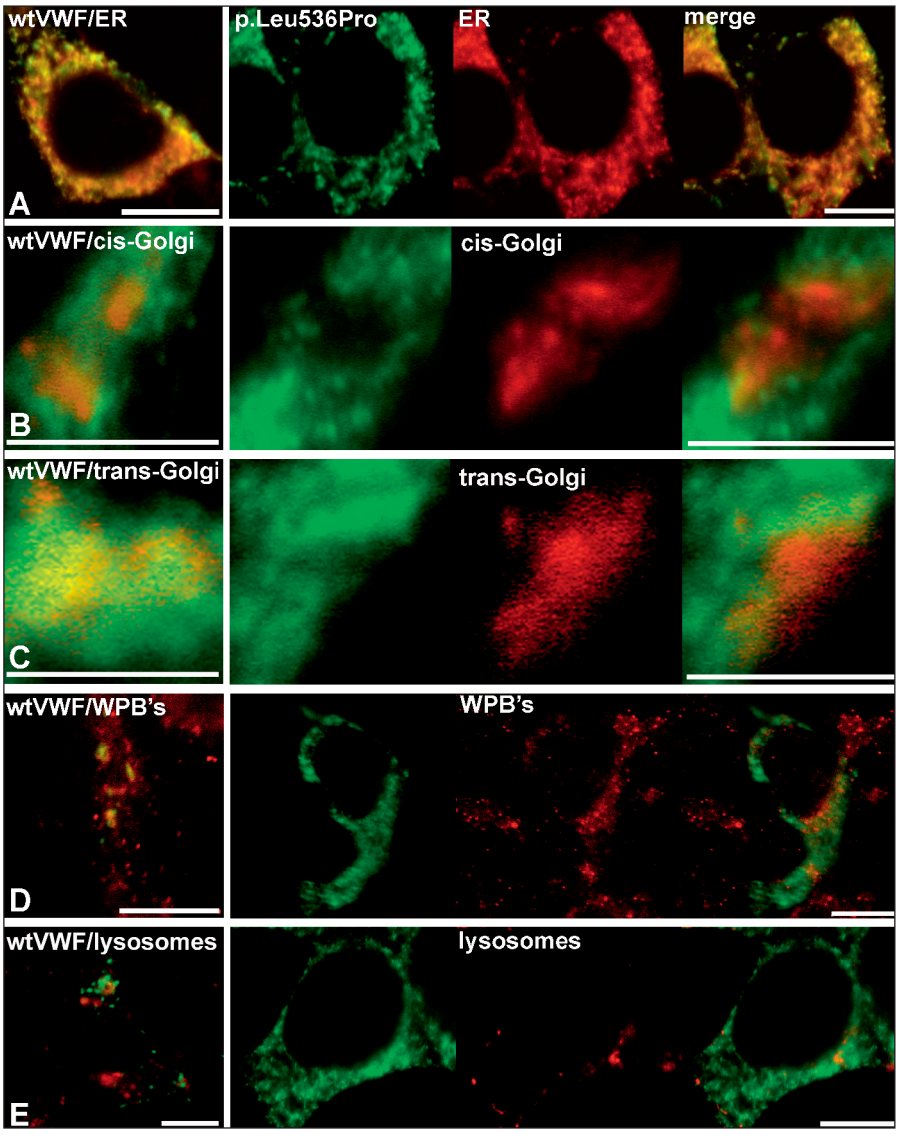

Figure 4: Intracellular localisation of VWD type 2A/IIC mutants in HEK293 cells. VWD 2A/IIC-associated VWF mutant p.Leu536Pro was transiently expressed in HEK293 cells. 48 h after transfection cells were fixed and p.Leu536Pro as well as subcellular compartments were detected by indirect immunofluorescence employing anti-VWF and antibodies against marker proteins. Anti-PDI for the ER (A), anti-GOLPH4 for cis-Golgi (B), anti-TGN46 for trans-Golgi (C), anti-Rab27a for pseudo-Weibel-Palade bodies (D) and anti-LAMP2 for lysosomes (E). To illustrate the altered mutant localisation compared to wtVWF, the left-hand column shows an overlay of immunofluorescent detection of wtVWF and the indicated cellular compartments. Three independent experiments for each mutant and for each subcellular compartment were performed. Scale bars represent 10 µm.

any platelet surface coverage (< 1% each). Mutant p.Tyr1146Cys led to an intact but decreased platelet binding with a resulting relative surface coverage of 39 ± 5% (►Figure 6A).

Functional characterisation of VWF mutant-affected string formation under flow conditions

Shear-induced unfolding of the biopolymer VWF leads to an interaction of the exposed VWF A1 domain with GPIb on the platelets' surface and to a polymerisation to ultralarge VWF fibres at the vessel wall in the absence of ADAMTS13. To further functionally characterise the VWF mutants we focused on their ability to form an intact platelet binding string pattern near the vessel wall. Therefore, we performed microfluidic experiments under substitution of the soluble plasma VWF fraction with physiologic concentration of the VWF mutants (10 µg/ml) in a wide ranged high-shear regime. In the presence of only wtVWF in the supernatant we observed platelet decorated ultra-large VWF fibres at the wtVWF biofunctionalised channel surface at shear rates ≥ 2,500 s^{-1}, impressively increasing in size and platelet decoration with higher shear rates up to a length of several 100 µm (►Figure 6B, wtVWF). As expected, no string-like structures were found in the absence of soluble VWF (►Figure 6B, w/o).

Compared to wtVWF all VWF mutants showed lesser extent of platelet binding and string formation but with highly distinctive patterns (►Figure 6B): The VWD type 2A/IIC mutant p.Leu536Pro led to erratically distributed clotty fibres at 5,000 s^{-1} and 10,000 s^{-1}, whereas p.Gly550Arg only formed a few single fibres with low platelet decoration at 10,000 s^{-1}.

Also the type 2A/IID mutants showed different characteristics. At 5,000 s^{-1} p.Cys2773Arg and p.Ser2775Cys formed short strings decorated with up to three platelets, at 10,000 s^{-1} p.Cys2773Arg built regularly distributed but filigree strings (see Suppl. Video 1, available online at www.thrombosis-online.com) and p.Ser2775Cys also showed residual formation of less filigree and

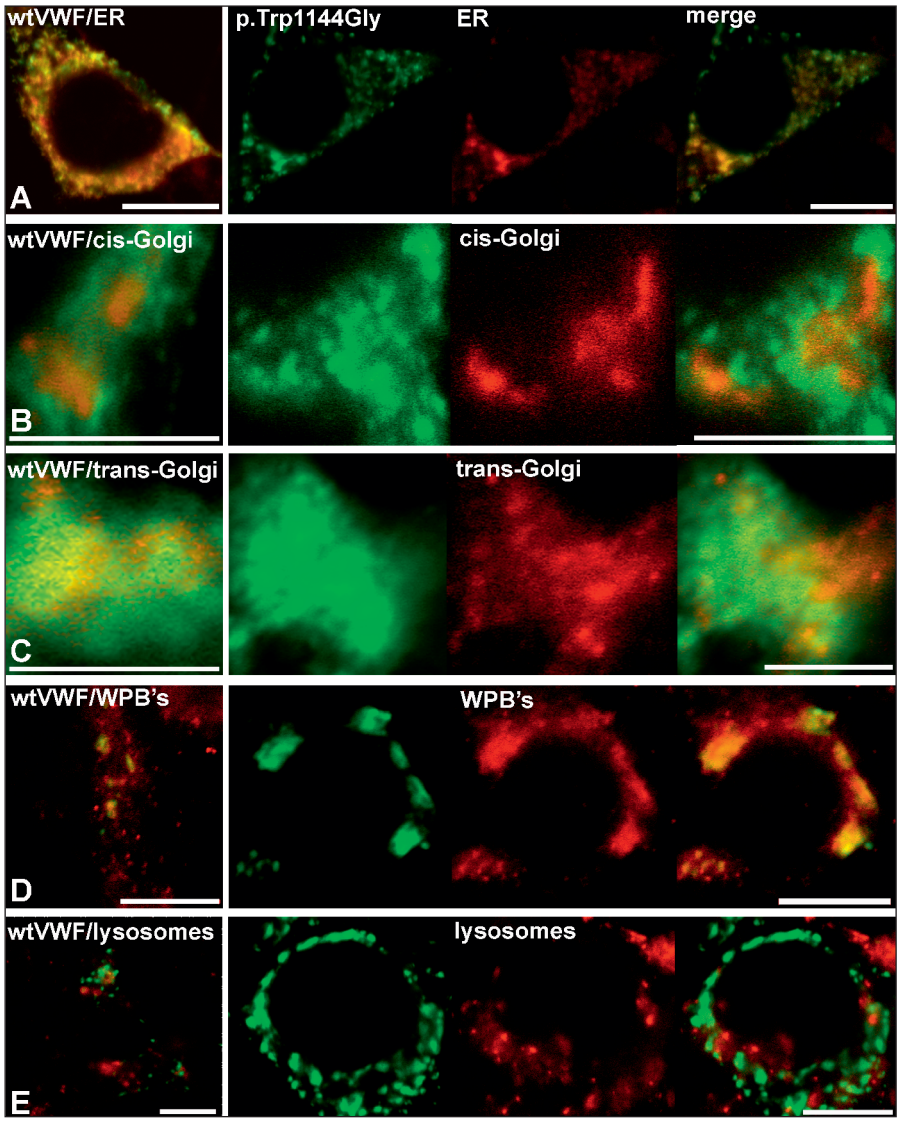

Figure 5: Intracellular localisation of VWD type 2A/IIE mutants in HEK293 cells. VWD 2A/IIE-associated VWF mutant p.Trp1144Gly was transiently expressed in HEK293 cells. 48 h after transfection cells were fixed and p.Trp1144Gly as well as subcellular compartments were detected by indirect immunofluorescence employing anti-VWF and antibodies against marker proteins. Anti-PDI for the ER (A), anti-GOLPH4 for cis-Golgi (B), anti-TGN46 for trans-Golgi (C), anti-Rab27a for Weibel-Palade bodies (D) and anti LAMP2 for lysosomes (E). To illustrate the enhanced localisation of the mutant in pseudo-WPB's compared to wtVWF, the left-hand column shows an overlay of immunofluorescent detection of wtVWF and the indicated cellular compartments. Three independent experiments for each mutant and for each subcellular compartment were performed. Scale bars represent 10 µm.

more clotty strings. p.Cys2771Arg completely failed to form platelet binding strings.

The type 2A/IIE mutant p.Trp1144Gly built regular platelet binding strings at the same shear rates as wtVWF but of lower quantity and platelet binding capacity. p.Cys1169Trp showed few filigree strings comparable to p.Cys2773Arg only at a shear rate of 10,000 s^{-1}. The mutant p.Tyr1146Cys exhibited a divergent pattern compared to the other type 2A/IIE mutants. In the whole range from lower to higher shear rates this mutant formed conglomerates of adhered platelets instead of impressive strings.

These data show clear differences in the string formation capability also within the subgroups of VWD/2A.

Characteristics of VWF mutants in polymer-platelet-aggregate formation

At high shear rates, VWF (polymer) and platelets form reversible polymer-colloid aggregates rolling at a VWF biofunctionalised surface (32). This rolling aggregate formation occurs when the VWF concentration in whole blood is elevated to pathophysiological levels of 50 µg/ml. By supplementing wtVWF or VWF mutants in whole blood to this concentration, we investigated the functional characteristics of VWF mutants in rolling aggregate formation. This process was quantified by determination of the critical shear rate at which first aggregates were observable. ►Figure 7A demonstrates highlighted sequences of reflection interference contrast microscopy (RICM) time-lapse images to illustrate the process of aggregate formation (see also Suppl. Videos 2 and 3, available online at www.thrombosis-online.com).

Using supplementary wtVWF first small conglomerates were detected at a shear rate of 3,000 s^{-1}. Stable aggregates appeared at 4,000 s^{-1}, growing in size and incidence with higher shear rates (►Figure 7B). Interestingly, none of the investigated mutants behaved like wtVWF: The VWD type 2A/IID mutants p.Cys2773Arg (Suppl. Video 4, available online at www.thrombosis-online.com) and p.Cys2771Arg led to a reduction of the critical shear rate. Al-

ready at 1,000 s^{-1} first small aggregates were generated with a remarkable high incidence. But with an increase of shear these aggregates remained small and round-shaped. In contrast, p.Ser2775Cys failed to induce rolling aggregate formation as well as the VWD type 2A/IIE mutant p.Tyr1146Cys. The other IIE mutant p.Cys1169Trp formed first small aggregates at a high shear rate of 5,000 s^{-1}. Due to impaired secretion a concentration of 50 µg/ml of mutants p.Leu536Pro, p.Gly550Arg and p.Trp1144Gly was not available for these experiments.

Taken together, these distinct characteristics in polymer-platelet aggregate formation open the possibility to mechanistically analyse the VWD subtypes regarding their functional defects matching with the clinical implications and individual patient´s symptoms.

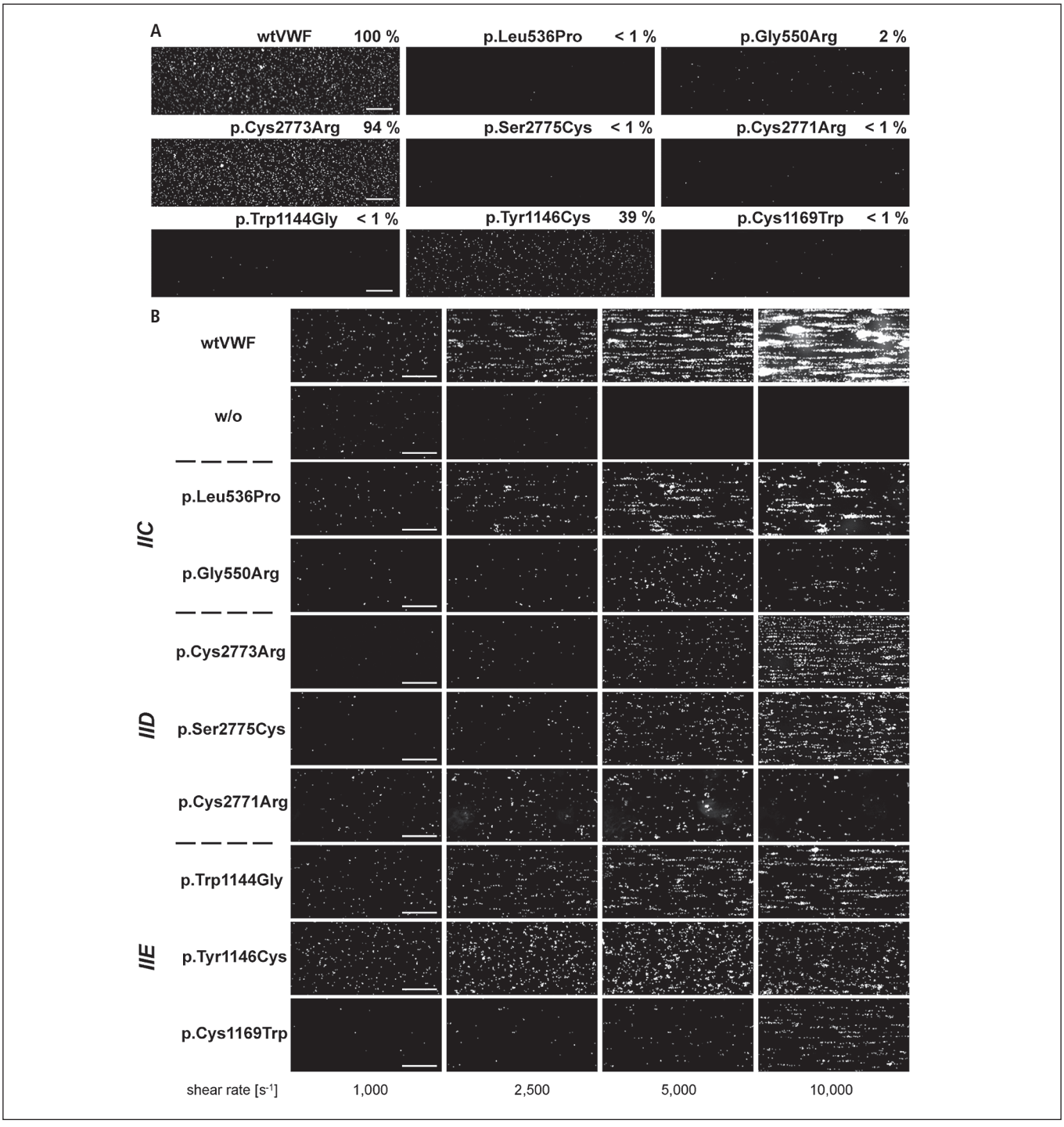

Discussion

For VWD type 2A/IIC, IID and IIE mutants, we found a correlation between the mutated domain, intracellular localisation of the mutant and their respective multimer patterns that is characteristic for each subtype and further mirrors the severity of the mutation-induced defect in intracellular processing within each phenotype.

Our data of the investigated type 2A/IID mutants confirm that mutations within the CK domain of VWF lead to C-terminal dimerisation defects with differences in severity (25, 26, 33) but they also broaden our understanding of the cysteine residues involved in dimerisation. In detail, we investigated the cysteine inducing mutation, p.Ser2775Cys and the two previously described cysteine abolishing mutations p.Cys2771Arg (34) and p.Cys2773Arg (25). It has been shown that the latter two VWF mutants form N-terminal dimers to different extent (35), presumably by using unpaired cysteine residues in the multimerisation domain for interchain disulphide bonds thereby inhibiting multimerisation. Our multimer analysis confirmed these data and additionally showed that p.Ser2775Cys is only able to form dimers plus tetramers. This loss of C-terminal dimerisation could be the reason for the increase in cytosolic localisation of p.Cys2771Arg and p.Ser2775Cys, probably due to a decreased processing time in the ER. Normal Golgi localisation supports the hypothesis that these mutants do follow the regular pathway through the Golgi-apparatus where they become N-terminally dimerised. Together with our MD simulations, which were in high accordance with our experimental findings (►Figure 3), our data suggest that dimerisation is favoured in compact conformations and blocked in extended conformations. Mutant p.Ser2775Cys features more extended conformations while p.Cys2773Arg displayed ambiguous VWF dimer formation, which could be attributed to the alternating structures of CK observed in the simulations. Therefore, p.Cys2773Arg has the least effect on dimerisation which is surprising since it has been suggested that the CK domains dimerise exclusively through Cys2773, assuming arrangement in the same orientation as the two domains of TGF-β2 (16, 17). Our data indicate that Cys2771 also plays a crucial role in dimerisation, presumably by linking the two CK domains. The almost complete abolishment of dimer formation by p.Ser2775Cys indicates that addition of another unpaired cysteine may increase formation of alternate intra-domain disulphide bonds (Suppl. Figure 5, available online at www.thrombosis-online.com), which may alter the composition of inter-domain disulphide bonds compared to wtVWF. [The recent crystal structure of the CK domain (27) confirms our data. It was shown that the CK domains are dimerised by disulphide bonds between Cys2771-Cys2773', Cys2773-Cys2771' and Cys2811-Cys2811'. Therefore, single mutation of Cys2771 or Cys2773 both abolish two crucial disulphide bonds. Mutation of Cys2771 seems also to abolish the third disulphide bond between the two Cys2811 residues. One possible explanation might be that Cys2773 and Cys2811 form an intramolecular disulphide bond when Cys2771 is absent. Further we can now also hypothesise why mutation of Cys2773 might allow residual formation of small multimers: it seems that in some but not all monomers inter-molecular disulphide formation is still possible. But attachment of one monomer (that might have an intra-molecular bond between Cys2771 and Cys2811) would stop the multimerisation. This hypothesis is supported by the fact that in the patient additional bands due to odd-numbered multimers are visible. This could also explain why this mutant exhibits reduction of HMWM but normal intracellular localisation.][1] Mutation p.Ser2775Cys introduces an additional cysteine residue and therefore leads to a dimerisation defect through another mechanism. Probably the new Cys2775 leads to unpredictable intra-molecular disulphide bonds that sometimes allow a minimal residual dimerisation leading to tetramers in the homozygous recombinant expression. Heterozygous expression in the patient leads to bleeding symptoms but normal or even increased VWF:Ag as well as collagen binding and no loss of HMWM (►Table 1). This mutation is a perfect example for the necessity of more extensive diagnostic tests in some cases. In case of this patient none of the conventional tests but only multimer analysis and our flow assay unmasked the structural and functional deficits, respectively.

Mutations in the pro-peptide are known to cause VWD type 2A/IIC with defective multimerisation and intracellular trafficking

Figure 6: Platelet binding capability of soluble VWF mutants and shear-induced fibre formation of immobilised VWF mutants. A) Microfluidic channels were biofunctionalised with either wtVWF or indicated VWF mutants and perfused with washed and stained platelets in a concentration of 200,000 per µl supplemented with 45% haematocrit at a shear rate of 500 s^{-1}. After 10 min of perfusion, adhesion to the VWF (wt or mutant) coated on the glass footprint of the channel was studied by fluorescence microscopy. In comparison to wtVWF biofunctionalisation type 2A/IIC VWD mutants p.Leu536Pro and p.Gly550Arg did not show relevant platelet binding. Mutant p.Cys2773Arg showed a platelet adhesion pattern comparable to wtVWF whereas the other type 2A/IID VWD mutants, p.Ser2775Cys and p.Cys2771Arg, failed to bind platelets. Biofunctionalisation with the type 2A/IIE mutants p.Trp1144Gly and p.Cys1169Trp did not show mentionable platelet adhesion yet p.Tyr1146Cys led to an intact but decreased platelet binding. Two independent experiments for each mutant were performed. B) To study string formation, channels were biofunctionalised with wtVWF and perfused with washed and stained platelets in a concentration of 200,000 per µl supplemented with 45% haematocrit at various shear rates in the range of 1,000 s^{-1} to 10,000 s^{-1} for 1 min each. Focusing on the ability to form an intact platelet binding string pattern, we found platelet decorated ultra-large VWF fibres at the wtVWF biofunctionalised channel surface, impressively increasing in size and platelet decoration with higher shear rates, whereas no string-like structures were found in the absence of soluble VWF. The type 2A/IIC VWD mutant p.Leu536Pro led to erratically distributed clotty fibres and p.Gly550Arg only formed single fibres with low platelet decoration at high shear rates. The type 2A/IID mutant p.Ser2775Cys formed short strings, p.Cys2773Arg built regularly distributed but filigree platelet decorated string-like structures and p.Cys2771Arg failed to form platelet binding strings. The type 2A/IIE mutant p.Trp1144Gly build regular platelet binding strings but of lower quantity and platelet binding capacity. p.Cys1169Trp showed filigree strings comparable to p.Cys2773Arg under high-shear conditions and p.Tyr1146Cys formed conglomerates of adhered platelets instead of impressive strings. At least three independent experiments for each mutant were performed. Scale bars represent 100 µm.

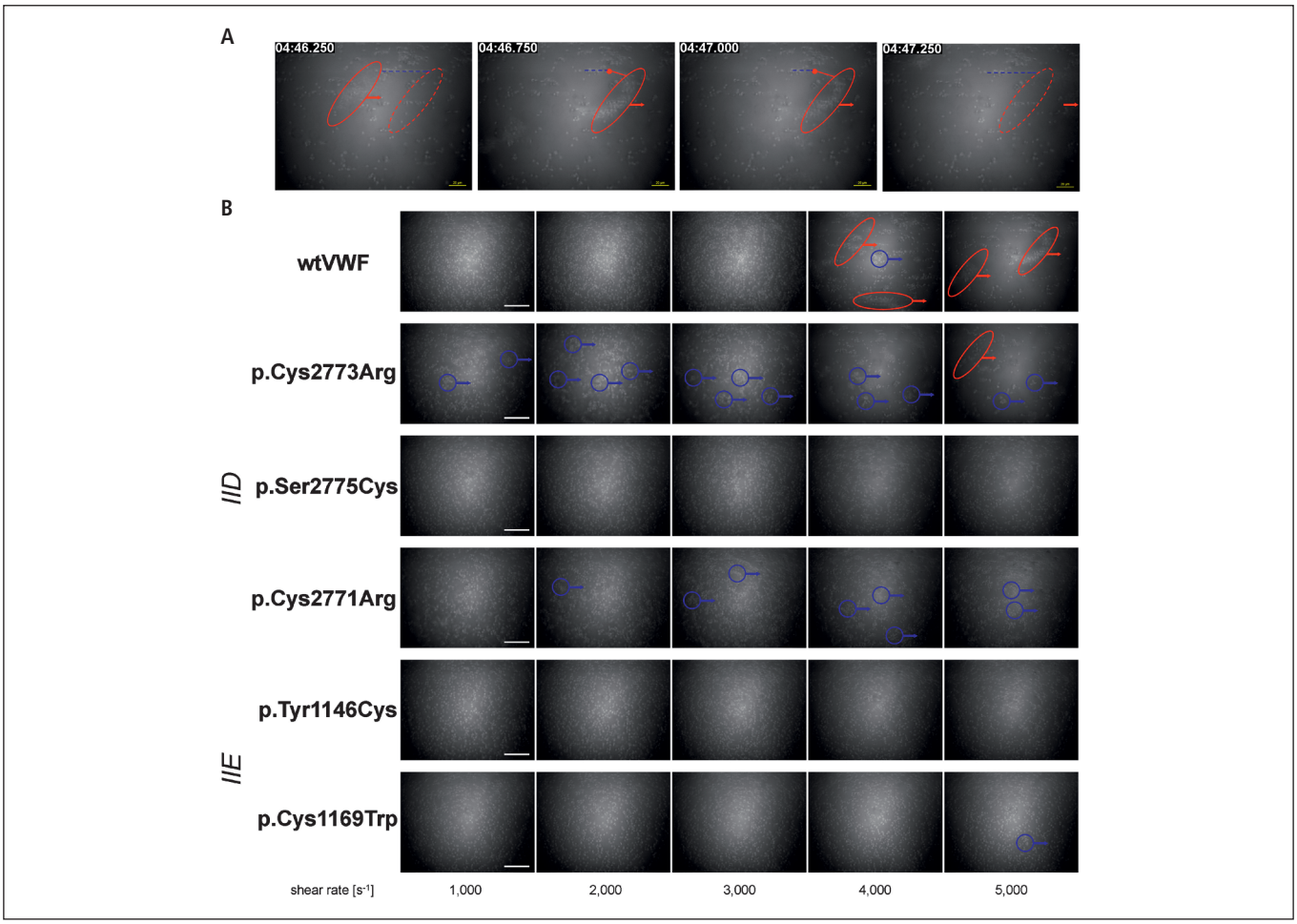

Figure 7: Formation of polymer-platelet-aggregates and effect of VWF mutants on formation of rolling aggregates under high shear conditions. To investigate rolling aggregate formation, channels were bio-functionalised with wtVWF and perfused with native whole blood supplemented with wtVWF or indicated VWF mutant to 50 µg/ml. For determination of the critical shear rate, the flow was consecutively increased from 1,000 s^{-1} to 5,000 s^{-1} for 1 min each and live cell RICM videos were taken with 2 frames/s. Critical shear rate was defined as the shear rate at which the first rolling aggregates emerged that contained at least 15 platelets. Under high-shear conditions in whole blood with added wtVWF, time-lapse images of polymer-platelet-aggregate formation in the range of a 1-second period are performed. A) The present position of an aggregate is highlighted with a red oval and the prospective short-termed stationary position is marked by a red dashed oval, whereupon a red arrow indicates the locomotion direction. On a platelet decorated string-like VWF structure (blue dashed line) the aggregate builds a rapid anchor-point (red dot) and deforms the VWF string (red line). After detachment, the aggregate moves forward out of the field of view. For a short video presentation of this process see also Suppl. Video 2 (available online at www.thrombosis-online.com). Time frame is indicated, scale bars correspond to 20 µm. B) Using supplementary wtVWF under whole blood conditions, first aggregates emerged at a shear rate of 4,000 s^{-1}, growing in size and incidence with higher shear. The mutants p.Cys2773Arg and p.Cys2771Arg led to a reduction of the critical shear rate indicating a gain-of-function, but rolling aggregates remained small and round-shaped with an increase of shear. p.Ser2775Cys as well as p.Tyr1146Cys failed to induce rolling aggregate formation. p.Cys1169Trp formed first small aggregates at a high shear rate of 5,000 s^{-1}. Blue circles illustrate first conglomerate formation; red ovals indicate VWF-platelet-aggregates. At least three independent experiments for each mutant were performed. Scale bars represent 50 µm.

(36). Our investigation of newly identified mutant p.Leu536Pro from a compound heterozygous 2A/IIC patient (▶Table 1) and mutant p.Gly550Arg found in a homozygous patient (31) (▶Table 1) indicate that these effects might be caused by retention in the ER that could be due to misfolding.

Our VWD type 2A/IIE mutants exhibited normal ER and Golgi localisation indicating normal dimerisation as well as multimerisation. The increase in pseudo-WPB size and quantity suggest increased storage and a secretion defect that was further confirmed by reduction of PMA-dependent and -independent secretion. Only mutant p.Cys1169Trp could be released to the same extent as wtVWF. These data are in line with the observation that in the compound heterozygous patient with VWF:Ag of 9% (see ▶Table 1), VWF:Ag raised to 26% by DDAVP with subsequent rapid decrease in VWF:Ag within 2 h to 13% (personal communication by H. Lenk). These data further suggest a significant decrease of the VWF mutant's half-life.

In conclusion, we show that for type 2A IIC, IID, and IIE mutations a correlation exists between the domain that carries the mutation and the defect in biosynthesis. For each mutant the severity of the processing defect correlates with the alteration in the intracellular localisation and with the reduction of HMWM observed in the particular VWF mutant multimer pattern. Mutations in the dimerisation domain, that lead to reduction of multimer size to dimers and tetramers increased cytosolic localisation, indicating faster trespassing through the ER, mutations in the propeptide lead to retention in the ER and mutations in the D3 domain cause retention in WPB's.

Interestingly, no correlation exists between the 2A phenotype and effect on the shear flow-dependent functions of VWF: Under shear flow conditions with normal physiological concentration of the mutants we observed three groups of string formation defects independent of the VWD subtypes: p.Leu536Pro (subtype 2A/IIC) and p.Trp1144Gly (2A/IIE) exhibited the mildest phenotype with slightly reduced string formation with onset at the same shear rates as wtVWF (2,500 s^{-1}). p.Gly550Arg (2A/IIC), p.Cys2773Arg (2A/IID), p.Ser2775Cys (2A/IID) and p.Cys1169Trp (2A/IIE) started to form tiny strings decorated with three platelets at 5,000 s^{-1} and filigree, pearls-on-a-string-like decorated fibres at 10,000 s^{-1}.

p.Tyr1146Cys (2A/IIE) completely failed to form strings at any shear rate. The additional cysteine residue could result in formation of disulphide bonds which are usually not formed in wtVWF. The alteration of the mutant VWF secondary structure by these new bonds seems to inhibit normal processing, string formation and platelet binding.

In the string formation assay mutant p.Cys2771Arg (2A/IID) was also completely incapable to form strings at physiological concentration but additionally exhibited formation of small conglomerates with platelets already initiated at a shear rate of 1,000 s^{-1}, indicating a gain-of-function through better accessibility of the platelet binding site in p.Cys2771Arg dimers.

While still able to form small strings p.Cys2773Arg also exhibited a gain-of-function at high pathophysiological concentration by binding platelets already at 1,000 s^{-1}.

p.Cys1169Trp and p.Tyr1146Cys failed to form platelet conglomerates at all shear rates investigated. It further has to be taken into consideration that some of the aforementioned mutations exhibited a decreased secretion as shown in Suppl. Figure 6 (available online at www.thrombosis-online.com), presumably resulting in a reduced VWF concentration in the plasma of affected patients. However, some of the patients show increase of secretion after treatment with DDAVP. In such cases the shear-dependent dysfunction of the VWF mutants could still essentially contribute to the patient's phenotype. We show here that single missense mutations within VWF create a wide range of both processing and functional defects which can only comprehensively be described by an approach that combines static as well as microfluidic assays. Resulting data significantly increase insight into the different phenotypes of VWD 2A patients because they offer the possibility to explain variations in the patients' symptoms on a molecular level. For example, our patient with mutation p.Tyr1146Cys exhibited more severe bleeding symptoms than most other 2A/IIE patients, including epistaxis, haematoma, menorrhagia, haematuria, intestinal bleeding, and even joint bleeding requiring prophylaxis (31). Our findings that mutant p.Tyr1146Cys completely failed to form VWF strings and platelet conglomerates at all shear rates now explain these symptoms which cannot be explained by multimer analysis and other static tests: In contrast to the other investigated IIE mutants this mutant does not have residual platelet binding capacity and therefore presumably induces more severe bleeding. Additionally, our data could open new possibilities for diagnosis and treatment options for VWD 2A patients. In general 2A patients are treated with plasma-derived VWF which might not always be necessary. In case of mutations p.Cys1169Trp we were able to show that this mutant can still be released by stimulation and that is does have residual string formation and platelet binding activity. In case of this patient treatment with DDAVP was suc-

Table 1: Phenotypic parameters for the patients whose multimer patterns are shown in Figure 2 are given in %. * indicates that the patient was not heterozygous for the mutation: p.Gly550Arg: homozygous; p.Leu536Pro: compound heterozygous with p.Ile94Asn; p.Cys1169Trp: compound heterozygous with null allele c.2435delC.

Mutation	Phenotype	VWF:Ag	CB	R:Co	FVIII	Reference
p.Cys2773Arg	2A/IID	119	7	64	90	25
p.Ser2775Cys	2A/IID	184	193			novel
p.Cys2771Arg	2A/IID	110	32			32
p.Gly550Arg*	2A/IIC	59	< 2			29
p.Leu536Pro*	2A/IIC	23	2			novel
p.Trp1144Gly	2A/IIE	27	12	19	27	28
p.Tyr1146Cys	2A/IIE	20	16	7	1	28
p.Cys1169Trp*	2A/IIE	9		4		28

What is known about the topic?

- VWD type 2A phenotypes IIC, IID and IIE are caused by mutations in the propeptide, the CK-domain and the D3-domain of VWF, respectively.
- Mutations associated with VWD type 2A phenotypes IIC, IID and IIE can alter processing, trafficking and secretion of VWF.

What does the paper add?

- The wide range of defects induced by VWD type 2A phenotypes IIC, IID and IIE VWF mutants is comprehensively described by an approach that combines intracellular localisation studies, multimer analyses and microfluidic assays.
- Molecular dynamics simulations add to the understanding of carboxy-terminal dimer formation.
- Our new microfluidic screening method provides the possibility to extend VWD diagnostics to shear flow-dependent VWD subtypes which are currently not detectable.

cessfully applied. Therefore, adequate treatment options can accurately be chosen, when secretion and shear-activated properties of the mutants are determined.

In conclusion, here, we fully describe shear-dependent and -independent effects of type 2A IIC, IID and IIE mutations which have severe consequences during the "day in the life" of these mutants; namely beginning with their intracellular synthesis, processing and trafficking to their shear-dependent functions in the circulation. More importantly, we developed a VWD screening method that could, without any further modifications, be used with patient blood samples to complete VWD diagnosis covering all shear-dependent VWF functions which are not covered by current state-of-the-art static VWD diagnostics. It could also provide the possibility to extend VWD diagnostics to new shear-flow-dependent VWD subtypes which are currently not detectible by the static assays.

Acknowledgements

We thank Prof. B. de Groot for providing the PLS-FMA tool, U. Klemm for data analysis and statistics, Gesa König and Annika Stüven for technical assistance, and Dr. H. Lenk for providing DDAVP data.

Conflicts of interest

None declared.

References

1. Haberichter SL, Fahs SA, Montgomery RR. von Willebrand factor storage and multimerization: 2 independent intracellular processes. Blood 2000; 96: 1808-1815.
2. Wagner DD. Cell biology of von Willebrand factor. Annu Rev Cell Biol 1990; 6: 217-246.
3. Metcalf DJ, Nightingale TD, Zenner HL, et al. Formation and function of Weibel-Palade bodies. J Cell Sci 2008; 121: 19-27.
4. Alexander-Katz A, Schneider MF, Schneider SW, et al. Shear-flow-induced unfolding of polymeric globules. Phys Rev Lett 2006; 97: 138101.
5. Schneider SW, Nuschele S, Wixforth A, et al. Shear-induced unfolding triggers adhesion of von Willebrand factor fibers. Proc Natl Acad Sci USA 2007; 104: 7899-7903.
6. Singh I, Themistou E, Porcar L, et al. Fluid shear induces conformation change in human blood protein von Willebrand factor in solution. Biophys J 2009; 96: 2313-2320.
7. Cheng H, Yan R, Li S, et al. Shear-induced interaction of platelets with von Willebrand factor results in glycoprotein Ibalpha shedding. Am J Physiol Heart Circ Physiol 2009; 297: H2128-2135.
8. Ruggeri ZM. Structure of von Willebrand factor and its function in platelet adhesion and thrombus formation. Best Pract Res Clin Haematol 2001; 14: 257-279.
9. Schneppenheim R, Budde U. von Willebrand factor: the complex molecular genetics of a multidomain and multifunctional protein. J Thromb Haemost 2011; 9 (Suppl 1): 209-215.
10. Brehm MA, Schenk TMH, Zhou X, et al. Intracellular localization of human Ins(1,3,4,5,6)P-5 2-kinase. Biochem J 2007; 408: 335-345.
11. Budde U, Schneppenheim R, Eikenboom J, et al. Detailed von Willebrand factor multimer analysis in patients with von Willebrand disease in the European study, molecular and clinical markers for the diagnosis and management of type 1 von Willebrand disease (MCMDM-1VWD). J Thromb Haemost 2008; 6: 762-771.
12. Budde U, Schneppenheim R, Plendl H, et al. Luminographic detection of von Willebrand factor multimers in agarose gels and on nitrocellulose membranes. Thromb Haemost 1990; 63: 312-315.
13. Schneppenheim R, Plendl H, Budde U. Luminography-an alternative assay for detection of von Willebrand factor multimers. Thromb Haemost 1988; 60: 133-136.
14. Daopin S, Piez KA, Ogawa Y, et al. Crystal structure of transforming growth factor-beta 2: an unusual fold for the superfamily. Science 1992; 257: 369-373.
15. Meitinger T, Meindl A, Bork P, et al. Molecular modelling of the Norrie disease protein predicts a cystine knot growth factor tertiary structure. Nat Genet 1993; 5: 376-380.
16. Zhou YF, Eng ET, Zhu J, et al. Sequence and structure relationships within von Willebrand factor. Blood 2012; 120: 449-458.
17. Katsumi A, Tuley EA, Bodo I, et al. Localization of disulfide bonds in the cystine knot domain of human von Willebrand factor. J Biol Chem 2000; 275: 25585-25594.
18. Hess B, Kutzner C, van der Spoel D, et al. GROMACS 4: Algorithms for highly efficient, load-balanced, and scalable molecular simulation. J Chem Theory Comput 2008; 4: 435-447.
19. Van der Spoel D, Lindahl E, Hess B, et al. GROMACS: Fast, flexible, and free. J Comput Chem 2005; 26: 1701-1718.
20. Krivobokova T, Briones R, Hub JS, et al. Partial least-squares functional mode analysis: application to the membrane proteins AQP1, Aqy1, and CLC-ec1. Biophys J 2012; 103: 786-796.
21. Rickham PP. Human Experimentation. Code of Ethics of the World Medical Association. Declaration of Helsinki. Br Med J 1964; 2: 177.
22. De Ceunynck K, Rocha S, Feys HB, et al. Local elongation of endothelial cell-anchored von Willebrand factor strings precedes ADAMTS13 protein-mediated proteolysis. J Biol Chem 2011; 286: 36361-36367.
23. Schneider CA, Rasband WS, Eliceiri KW. NIH Image to ImageJ: 25 years of image analysis. Nat Methods 2012; 9: 671-675.
24. dos Santos SM, Klinkhardt U, Schneppenheim R, et al. Using ImageJ for the quantitative analysis of flow-based adhesion assays in real-time under physiologic flow conditions. Platelets 2010; 21: 60-66.
25. Schneppenheim R, Brassard J, Krey S, et al. Defective dimerization of von Willebrand factor subunits due to a Cys-> Arg mutation in type IID von Willebrand disease. Proc Natl Acad Sci USA 1996; 93: 3581-3586.
26. Wang JW, Groeneveld DJ, Cosemans G, et al. Biogenesis of Weibel-Palade bodies in von Willebrand's disease variants with impaired von Willebrand factor intrachain or interchain disulfide bond formation. Haematologica 2012; 97: 859-866.
27. Zhou YF, Springer TA. Highly reinforced structure of a C-terminal dimerization domain in von Willebrand factor. Blood 2014; Epub ahead of print.
28. Allen S, Abuzenadah AM, Hinks J, et al. A novel von Willebrand disease-causing mutation (Arg273Trp) in the von Willebrand factor propeptide that results in defective multimerization and secretion. Blood 2000; 96: 560-568.
29. Gaucher C, Dieval J, Mazurier C. Characterization of von Willebrand factor gene defects in two unrelated patients with type IIC von Willebrand disease. Blood 1994; 84: 1024-1030.
30. Schneppenheim R, Thomas KB, Krey S, et al. Identification of a candidate missense mutation in a family with von Willebrand disease type IIC. Hum Genet 1995; 95: 681-686.
31. Schneppenheim R, Michiels JJ, Obser T, et al. A cluster of mutations in the D3 domain of von Willebrand factor correlates with a distinct subgroup of von Willebrand disease: type 2A/IIE. Blood 2010; 115: 4894-4901.
32. Chen H, Fallah MA, Huck V, et al. Blood-clotting-inspired reversible polymer-colloid composite assembly in flow. Nat Commun 2013; 4: 1333.
33. Schneppenheim R, Budde U, Obser T, et al. Expression and characterization of von Willebrand factor dimerization defects in different types of von Willebrand disease. Blood 2001; 97: 2059-2066.
34. Enayat MS, Guilliatt AM, Surdhar GK, et al. Aberrant dimerization of von Willebrand factor as the result of mutations in the carboxy-terminal region: identification of 3 mutations in members of 3 different families with type 2A (phenotype IID) von Willebrand disease. Blood 2001; 98: 674-680.
35. Tjernberg P, Vos HL, Spaargaren-van Riel CC, et al. Differential effects of the loss of intrachain- versus interchain-disulfide bonds in the cystine-knot domain of von Willebrand factor on the clinical phenotype of von Willebrand disease. Thromb Haemost 2006; 96: 717-724.
36. Haberichter SL, Budde U, Obser T, et al. The mutation N528S in the von Willebrand factor (VWF) propeptide causes defective multimerization and storage of VWF. Blood 2010; 115: 4580-4587.

